The $\tilde{A}\,^2E$–$\tilde{X}\,^2A_1$ transition of monomethyl calcium: A rotational analysis

C. R. Brazier[a] and P. F. Bernath[b]
Department of Chemistry, The University of Arizona, Tucson, Arizona 85721

(Received 24 May 1989; accepted 14 July 1989)

The 0_0^0 band of the $\tilde{A}\,^2E$–$\tilde{X}\,^2A_1$ transition of $CaCH_3$ has been rotationally analyzed at Doppler-limited resolution by laser excitation spectroscopy. Observation of an internal perturbation in the excited state permitted simultaneous determination of both A' and A''. The ground-state molecular structure was found to be $R_{Ca\text{-}C} = 2.349(13)$ Å and $\theta_{H\text{-}C\text{-}H} = 105.6(28)°$ with $R_{C\text{-}H}$ fixed at 1.100(20) Å.

I. INTRODUCTION

The alkaline earth fluorides CaF (Refs. 1 and 2) and SrF (Refs. 3 and 4) were first studied in the late 1970s following the development of high-resolution dye laser spectroscopy. Since that the time the same techniques have been used to unravel the complex spectra of the isoelectronic hydroxide,[5–9] amide,[10,11] methyl,[12] and borohydride[13] derivatives. These species all have very similar spectra, characterized by a single $p \leftarrow s$ metal-centered transition in the yellow to red region of the spectrum. Initial spectra of monomethyl calcium[12] taken at 1 cm^{-1} resolution showed two electronic transitions, $\tilde{A}\,^2E$–$\tilde{X}\,^2A_1$ and $\tilde{B}\,^2A_1$–$\tilde{X}\,^2A_1$ near 6800 and 6250 Å, respectively. These are the two components of a p–s atomic transition in the C_{3v} symmetry of $CaCH_3$. In this paper we report a Doppler-limited rotational analysis of the 0_0^0 band of the $\tilde{A}\,^2E$–$\tilde{X}\,^2A_1$ transition of monomethyl calcium.

Very few molecules with ^2E electronic states have been studied so far. The first work was by King and Warren[14] on FSO_3 in 1969. The definitive study to date on a ^2E molecule is the microwave study of methoxy by Endo, Saito, and Hirota.[15] This proved very useful, both in this work and in our first study of a ^2E state, for an analysis of the $\tilde{A}\,^2E$–$\tilde{X}\,^2A_1$ transition of $SrOCH_3$ by O'Brien, Brazier, and Bernath.[16] Recently, there have been several laser-induced fluoresence studies by Miller and co-workers of species with ^2E electronic states, for example, CH_3O,[17,18] CH_3S,[19] and C_5H_5.[20] Further microwave studies have also been performed on the $^{13}CH_3O$ (Ref. 21) and CH_3S (Ref. 22) radicals.

II. EXPERIMENT

Monomethyl calcium was produced in a Broida-type oven[23] by the reaction of calcium vapor with a methyl-containing species. Calcium metal was resistively heated in an alumina crucible and the vapor entrained in a flow of argon carrier gas. Typical pressures were 5 Torr of argon and 2 Torr of oxidant with a slow flow through the system. Two metal alkyls, tetramethyl tin and dimethyl mercury, reacted readily with excited ^3P calcium atoms, produced by pumping the $^3P_1$–$^1S_0$ atomic transition at 6573 Å, to yield monomethyl calcium. Two dye lasers operating with DCM dye, one broadband (to excite the calcium atoms) and one single-frequency (Coherent 699-29) computer-controlled laser to probe the products, were focused into the oven. The laser beams were not precisely overlapped and the fluorescence from the probe laser was focused onto the entrance slit of a 0.64 m monochromator. The monochromator acted as a narrow-band filter to simplify the spectrum. The dispersed fluorescence was imaged onto an RCA C31034 phototube and after processing through photon-counting electronics recorded as a function of laser frequency using the Coherent Autoscan system. Generally, only the laser-induced fluorescence signal was recorded and the Autoscan calibration was checked each day by recording a section of the iodine spectrum and comparing this with the published line positions.[24,25]

III. RESULTS AND ANALYSIS

The low-resolution (1 cm^{-1}) spectrum of $CaCH_3$ is shown in Fig. 1. In the low-resolution analysis,[12] it was shown that the ν_6 sequence structure spacing matches the spin-orbit splitting. Thus, the 0_0^0 band of the $^2E_{1/2}$–$^2A_1$ spin component is the only band which is not overlapped by other strong sequence bands. This band centered at 6800 Å was analyzed first. At low resolution it is composed of two strong features which appear to be bandheads, but at Doppler-limited resolution there is no obvious structure or bandheads, merely a dense collection of rotational lines, about 100 per wave number. The expected branch pattern for a Hund's case (a) ^2E–$^2A_1$ transition is the same as that for a case (a) $^2\Pi$–$^2\Sigma^+$ transition but complicated by the presence of multiple subbands due to the K rotational structure. As observed for the isoelectronic hydroxides,[8,9] each spin–orbit component of the $^2\Pi$ state has six branches, $2P$, $2Q$, and $2R$, but spaced by approximately $-3B$, $-B(2)$, $+B(2)$, and $+3B$, rather than the conventional 0, $\pm 2B$. The bands also tend to be blue degraded, so we were disappointed not to find bandheads in the $-B$ branches because these had made the analysis possible in the case of $SrOCH_3$.[16]

The $\tilde{A}\,^2E$–$\tilde{X}\,^2A_1$ system of $CaCH_3$ is formally a perpendicular electronic transition, but if the orbital angular momentum about the top axis, ζ, is close to 1, i.e., it is not significantly quenched by the off-axis protons, then all of the subbands will have the same origin and the spectrum will look like a parallel transition. The observed energy levels are shown in Fig. 2, labeled by K, the angular momentum about the top axis excluding spin. In addition, the excited-state levels are labeled by K_R, the component of the rotational angular momentum, R, about the top axis. The levels are

[a] Current address: Air Force Astronautics Laboratory/LSX, Edwards Air Force Base, CA 93523.
[b] Alfred P. Sloan Fellow; Camille and Henry Dreyfus Teacher-Scholar.

 0021-9606/89/204548-07$02.10

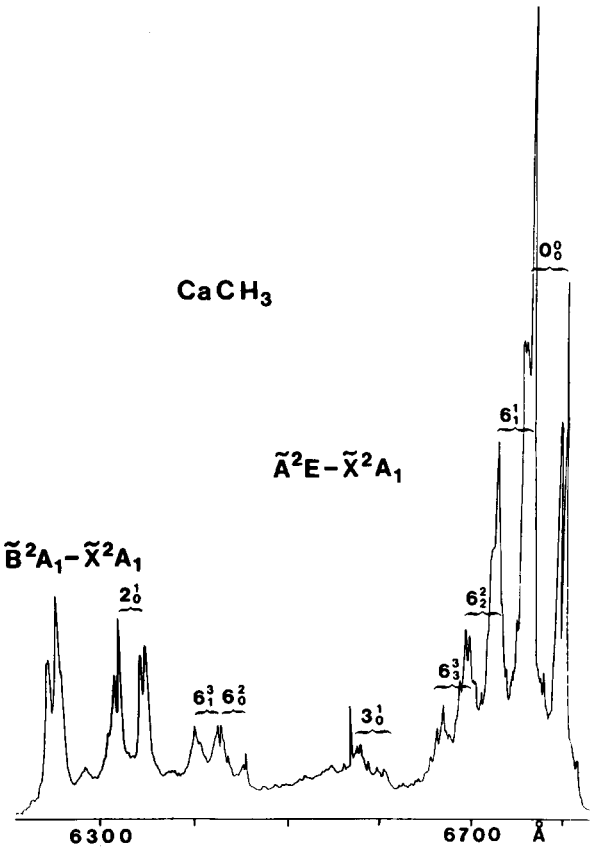

FIG. 1. Low-resolution laser excitation spectrum of the $\tilde{A}\,^2E$–$\tilde{X}\,^2A_1$ and $\tilde{B}\,^2A_1$–$\tilde{X}\,^2A_1$ systems of $CaCH_3$. The $^2E_{1/2}$–$^2A_1$ component of the 0_0^0 band is clear at 6800 Å, while the $^2E_{3/2}$–$^2A_1$ component is overlapped by the 6_1^1 sequence band.

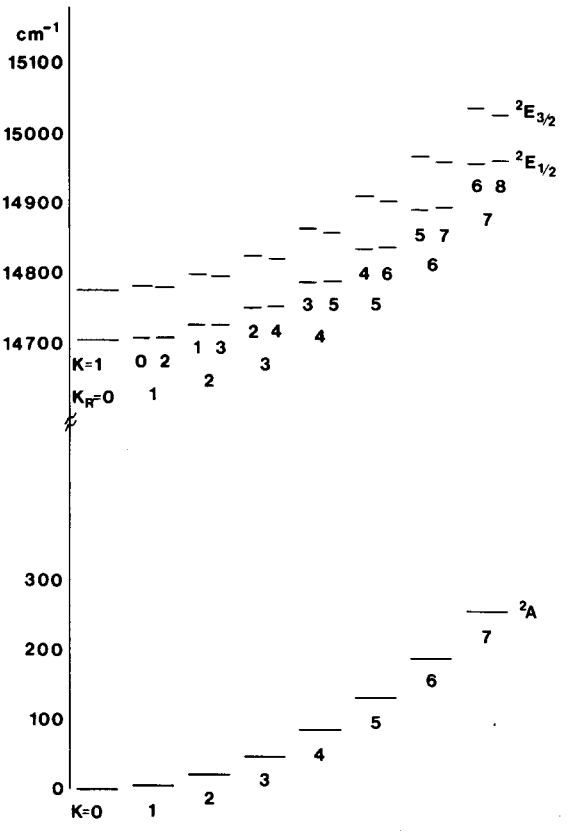

FIG. 2. Energy-level diagram for the K stacks of the 0_0^0 band of the $\tilde{A}\,^2E$–$\tilde{X}\,^2A_1$ system of $CaCH_3$. The lowest-J level which is present for all four stacks of a given K_R in the excited state is plotted. In the ground state, the level $N = K$ is given in each case.

also ordered by K_R, rather than by K as, for example, in Herzberg,[26] because this gives a much clearer picture of the level pattern in this case. The value of K_R is the same for this case as the quantum number G introduced by Hougen[27] and discussed by Herzberg.[26] The reason for the similarity of the energy-level patterns in the ground and excited states is clear from the energy-level expression for the K states:

$$E = (A - B)K^2 - 2A\zeta K. \tag{1}$$

It must be remembered that all of the quantities K, K_R, and ζ are signed and each level is in fact a degenerate pair, the other level is obtained by changing the sign of K, K_R, and ζ, except for $K = 0$ in the $\tilde{X}\,^2A_1$ state. For example, for $|K_R| = 3$, the possible levels are as follows (ignoring electron spin):

$$|K_R,\zeta,K\rangle = |3,1,4\rangle,|-3,-1,-4\rangle,|3,-1,2\rangle,|-3,1,-2\rangle,$$

with $K = K_R + \zeta$ and $|K| = |K_R| \pm 1$ in this case. The energies for the levels are then

$$E = (A - B)(K_R \pm \zeta)^2 - 2(\pm A\zeta)(K_R \pm \zeta)$$

if $A - B \simeq |A\zeta| \equiv A_{\text{eff}}$, then

$$E = A_{\text{eff}} K_R^2 - A_{\text{eff}}\,\zeta^2.$$

Because $K = K_R$ for the ground state and the only allowed transitions have $\Delta K_R = 0$, the subband origins are $T_K = T_0 + A'_{\text{eff}} K_R^2 - A'_{\text{eff}} \zeta^2 - A''_{\text{eff}} K_R^2$ and for $A'_{\text{eff}} \simeq A''_{\text{eff}}$, $T_K = T_0 - A_{\text{eff}}\,\zeta^2$. That is, to a first approximation all the subbands have the same origin.

In the absence of any signficant structure in the high-resolution total fluorescence spectrum, initial spectra were obtained by setting the monochromator to record emission in the strongest part of the $-B$ branch region and scanning in the $+B$ and $+3B$ branch regions. Due to the overlapping sequence structure, several different branches were apparent but one strong series of lines could be picked out clearly. By adjusting the monochromator wavelength, this series could be followed to high J and down to the origin. A section of this branch is shown in Fig. 3. This is the $+B$ branch and the spin-rotation splitting in the ground state is just becoming resolved. The monochromator enhances the lines of interest, but many other branches are still present as can be seen from the weak features in the base line and the high continuum level. This is because the different subbands have very similar rotational constants and origins, and thus are difficult to separate from one another.

The first lines were observed in all of the branches, although these were not completely obvious because weak features from other bands were frequently present which could have been additional lines. On the basis of the first lines, this band was tentatively assigned as the 4-3 subband which is expected to be one of the strongest subbands.

Other branches were observed while recording the 4-3

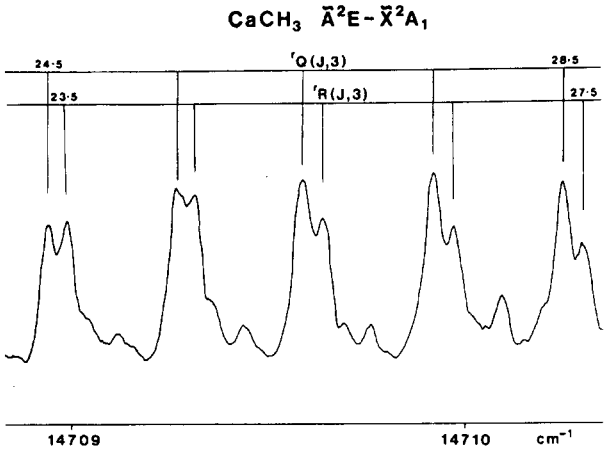

FIG. 3. High-resolution laser-induced fluorescence scan of part of the 4–3 subband in the $\tilde{A}\,^2E$–$\tilde{X}\,^2A_1$ component. This shows the $+B$ branch which is split into two by the ground-state spin-rotation interaction. Lines from other subbands also appear weakly between the 4–3 subband lines.

subband, and these could also be followed and the connecting branches found. Eventually, a clear pattern of subbands was discernable and the position of higher K subbands could be predicted. All of the bands with high statistical weight up to $K'' = 9$ were recorded, i.e., 8–9, 5–6, 2–3, 1–0, 4–3, 7–6, and 10–9. Subbands with $K'' = 0, 3, 6, 9, \ldots$ have statistical weights[26] twice that of the other K'' subbands. The assignments of these bands were consistent with the original assignment for the 4–3 subband. The subbands were initially fitted separately using a $^2\Pi$–$^2\Sigma^+$ Hamiltonian. The effects of "Λ-type doubling" or "l-type doubling" were observed in the 1–0 subband, the only one for which a significant splitting of the A_1 and A_2 (cf. e and f for $^2\Pi$) levels was expected. This splitting was observed as a combination defect because $K = 0$, in the $^2A_1$ ground state, has levels of alternately A_1 and A_2 symmetry. A systematic global perturbation of the higher K levels, particularly $K = 2$ and 4 ($K_R = 3$), in the excited state was observed. The levels could be fitted only by the inclusion of large higher-order centrifugal distortion terms such as H. This perturbation is due to the interaction of the states having the same K_R ($K = 2$ and $K = 4$ for $K_R = 3$) and was accounted for when the lines were fitted to a ^2E–^2A Hamiltonian by including the terms connecting the different K levels.

Having observed sufficient subbands in the $^2E_{1/2}$–$^2A_1$ component, a search was made near 6750 Å for the $^2E_{3/2}$–$^2A_1$ component. In this case some bandheads were observed, and when the lines for the individual subbands were recorded, the ground-state constants were the same as for the $^2E_{1/2}$–$^2A_1$ component. This confirms that the lines belong to the 0_0^0 vibrational band and not the 6_1^1 $^2E_{1/2}$–$^2A_1$ band which overlaps the origin band, as can be seen in Fig. 1. In this case, the 5–6, 2–3, 1–0, 4–3, 7–6, and 10–9 subbands were recorded.

All of the $^2E_{3/2}$–$^2A_1$ subbands could be fitted separately using a $^2\Pi$–$^2\Sigma^+$ Hamiltonian. In this case, the interaction between the levels arising from a common K_R is much weaker. The same term which causes the equivalent of Λ-doubling for $K = 1$ ($K_R = 0$) connects the pairs of levels for $K_R \neq 0$, and for the $^2E_{3/2}$ the Λ doubling is much smaller as is commonly seen in $^2\Pi$ states.

The only difficulty in the assignment of the $^2E_{3/2}$–$^2A_1$ spin component was deciding which of the bands originating in a given K for the ground state had $\Delta K = +1$ and which had $\Delta K = -1$. The problem is that both assignments can be fitted equally well, but with different constants. In most of the subbands the first lines were not clearly discernible because of the presence of additional overlapping lines from the 6_1^1 $^2E_{3/2}$–$^2A_1$ component. In this region, the line density is of the order of 300 per wave number. The most reasonable assignment was for the r-form subbands ($\Delta K = +1$) to go to lower energy from the origin and the p-form subbands ($\Delta K = -1$) to go to higher energy. This assignment was confirmed by comparing the relative intensities of the different branches with the formulas given by Brown.[28] In particular, for the p-form subbands the $-3B$ branch is strong while the $+3B$ is weak, and vice versa for r-form subbands. The difference in the subband degradation between the $^2E_{1/2}$–$^2A_1$ and $^2E_{3/2}$–$^2A_1$ components is caused by the large-ϵ_{aa} spin-rotation term which affects the two spin-orbit components by equal and opposite amounts.

A ^2E–^2A computer program was developed to fit the observed subbands simultaneously. The effective Hamiltonian of Brown[28] as extended by Hougen[29] was used. The matrix elements for both states were taken from Endo, Saito, and Hirota.[15] Some higher-order centrifugal distortion terms, which were needed because of the high rotational levels up to $J = 72.5$ and $K = 11$, were calculated from the matrix elements of Endo, Saito, and Hirota[15] by matrix multiplication. Due to the global perturbation effects in the $^2E_{1/2}$ levels, it was necessary to include the terms connecting levels having the same value of K_R. For example, $K = 4$ and 2 from $K_R = 3$. This is called the (2,2) interaction by Endo, Saito, and Hirota[15] because it arises in second order and connects states that have $K' + K'' = 2$ where K is a signed quantum number.

Note that Endo, Saito, and Hirota[15] use the shorthand notation

$$|J\ P\ S\ \Sigma;\pm\rangle = \frac{1}{\sqrt{2}}[\,|\Lambda = 1\rangle|S\Sigma\rangle|JPM_J\rangle \pm (-1)^{J-P+S-\Sigma}|\Lambda = -1\rangle \times|S,\ -\Sigma\rangle|J,\ -PM_J\rangle\,]$$

for the parity basis functions. Endo, Saito, and Hirota[15] use $\Lambda = \pm 1$ for our $\zeta = \pm 1$ and $P = K + \Sigma$ for the projection of the total angular momentum on the molecular symmetry axis. For example, with $K_R = 3$, eight basis functions arise:

$$|J,\ \Lambda = 1,\ K = 4,\ P = 4.5,\ \Sigma = \tfrac{1}{2}\rangle,$$
$$|J,\ \Lambda = 1,\ K = 4,\ P = 3.5,\ \Sigma = -\tfrac{1}{2}\rangle,$$
$$|J,\ \Lambda = -1,\ K = 2,\ P = 2.5,\ \Sigma = \tfrac{1}{2}\rangle,$$
$$|J,\ \Lambda = -1,\ K = 2,\ P = 1.5,\ \Sigma = -\tfrac{1}{2}\rangle,$$
$$|J,\ \Lambda = -1,\ K = -4,\ P = -4.5,\ \Sigma = -\tfrac{1}{2}\rangle$$
$$|J,\ \Lambda = -1,\ K = -4,\ P = -3.5,\ \Sigma = \tfrac{1}{2}\rangle,$$
$$|J,\ \Lambda = 1,\ K = -2,\ P = -2.5,\ \Sigma = -\tfrac{1}{2}\rangle,$$
$$|J,\ \Lambda = 1,\ K = -2,\ P = -1.5,\ \Sigma = \tfrac{1}{2}\rangle,$$

which are then converted to the eight parity combinations:

$$|J,\ K=4,\ P=4.5,\ \Sigma=\tfrac{1}{2};\ \pm\rangle,$$
$$|J,\ K=4,\ P=3.5,\ \Sigma=-\tfrac{1}{2};\ \pm\rangle,$$
$$|J,\ K=-2,\ P=-2.5,\ \Sigma=-\tfrac{1}{2};\ \pm\rangle,$$
$$|J,\ K=-2,\ P=-1.5,\ \Sigma=\tfrac{1}{2};\ \pm\rangle.$$

The definition of the parity-transformed basis function always has the $\Lambda=+1$ basis function first, which forces K and P to be negative with this notation when $|K|=|K_R|-1$.

The (2,2) interaction gives rise to the equivalent of "Λ-doubling" or "l-type doubling" in $K=1$ because this level can interact with itself. The higher order $(2,-1)$ and $(2,-4)$ terms, which connect together all values of K of a given symmetry, were neglected. One of the principle effects of these terms is to split the degeneracy of the A_1 and A_2 levels in $K=-2$. No sign of splitting or broadening was seen in the 2–3 subband, so the contribution from these terms must be small. Neglecting these terms allows the matrices to be reduced to a 4×4 block for each K_R in the excited state, making calculation of the energy levels much simpler.

Lines from the 13 subbands for both the $^2E_{1/2}$–^2A and $^2E_{3/2}$–^2A components were combined and fitted to the calculated ^2E–^2A transitions. The effective parallel nature of the transition means that the spacing of the K stacks in the ground and excited electronic states cannot be determined simultaneously. Initially, the ground-state A and D_K constants were held fixed to those for methyl fluoride.[30] This is one of the few methyl compounds for which the A and D_K rotational constants have been determined by observation of perturbation-allowed transitions.[30]

Initially, a small number of constants B, D_{NK}, D_N, and $(\epsilon_{bb}+\epsilon_{cc})/2$ for the ground state, and T, $a\zeta_c d$, A, $A\zeta_t$, $\eta_c\zeta_t$, $\eta_K\zeta_t$, B, D_K, D_{NK}, D_N, ϵ_{aa}, $(\epsilon_{bb}+\epsilon_{cc})/2$, ϵ_1, and h_1 for the excited state were used to fit the data. A reasonable fit of the order of 0.01 cm^{-1} could be obtained, although the residuals showed clear systematic trends.

Only the bands with high statistical weight ($K=0$, 3, 6, 9) in the ground state were recorded, but because of the very similar origins and rotational constants for all the subbands, many extra lines were observed in these spectra. These arise from the other weaker subbands, but without careful tracking of the branches or additional information, they are difficult to assign. However, the constants for the analyzed subbands could be used in conjunction with a spectrum prediction program to predict the lines of the weaker subbands. Based on this prediction, lines in the 9–10, 6–7, 4–5, 3–4, 1–2, 0–1, 2–1, 3–2, 5–4, 6–5, 8–7, and 11–10 subbands of the $^2E_{1/2}$–$^2A_1$ component and the 3–4, 1–2, 0–1, 2–1, and 3–2 subbands of the $^2E_{3/2}$–$^2A_1$ component were assigned.

At this point the solution to the previously unexplained doubling of the lines in the $-B$ and $+3B$ branches of the 1–0 band of the $^2E_{1/2}$–$^2A_1$ component was found. The origins of the 1–0 and 2–1 subbands were almost identical and the Λ-doubling effect in the excited state of the 1–0 subband results in the $-B$ and $+3B$ branches (which go to one Λ-doubling component) of the 1–0 band having almost exactly the same transition frequencies as the corresponding 2–1 band lines. Because these subbands have the same intensity, the observed lines were fitted to the average of the 1–0 and 2–1 calculated line positions when they were not clearly resolved.

At this stage it was observed that a small number of lines in the 2–1 and 3–4 subbands showed residuals which were characteristic of a perturbation. This is shown in Fig. 4. The deviations were quite small, of the order of 0.02 cm^{-1}, but because they were of the same magnitude and opposite sign in the two subbands, it was clear that an internal perturbation between the $K=2$ level for $^2E_{3/2}$ and $K=-3$ for $^2E_{1/2}$ was occurring. Figure 2 shows that these two levels lie close together. In order to make the crossing occur between $J=46.5$ and 47.5, the value of A'' was increased from 5.182 to 5.448 cm^{-1} with similar changes to A', $A'\zeta_t$, and T, to yield the original transition energies. The perturbation comes from the $(2,-1)$ term in the Hamiltonian with the selection rule $K_1+K_2=-1$. This was not originally included in the program because the matrices become too large to handle on a PC/AT computer. The interaction is only significant where the levels are close in energy, so the computer program was modified to treat the J values from 35.5 through 58.5 (12 on each side of the crossing) by including the $(2,-1)$ term. From Endo, Saito, and Hirota,[15] two terms contribute to the interaction, h_2 and ϵ_{2b}, but because only one crossing was observed only the combination $5h_2+\epsilon_{2b}$ can be determined. In addition, the absolute sign of the perturbation cannot be determined. With the inclusion of this interaction and allowing A'' to vary, the residuals were reduced to their expected values, as can be seen in Fig. 4. This was a very fortuitous observation because it permits the absolute determination of the A rotational constant. Only one perturbation was seen; therefore, the value of D_K'' was kept constrained to that for CH_3F (Ref. 30) in the final fit. Inspection of Fig. 2 shows that other crossings occur (for example, $K=-2$ and -4), but these levels have different symmetry, A_1/A_2 and E, respectively, so they cannot interact.

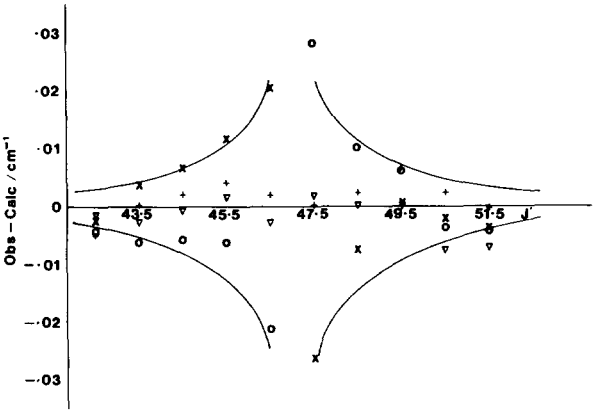

FIG. 4. The internal perturbation in the $\tilde{A}\,^2E$ state between $^2E_{1/2}$ ($K=-3$) and $^2E_{3/2}$ ($K=2$). The initial observed minus calculated data for the two bands (only lines from one branch in each case are shown) are given ($\times\Rightarrow{}^2E_{1/2}$, $K=-3$; $\circ\Rightarrow{}^2E_{3/2}$, $K=2$). Inclusion of the $(2,-1)$ perturbation term reduces the residuals to random values ($+\Rightarrow{}^2E_{1/2}$, $K=-3$; $\nabla\Rightarrow{}^2E_{3/2}$, $K=2$).

A total of 4030 lines[31] (of which 320 were given reduced weights due to blending) were included in the final fit. A fairly large number of constants, 32 in all, were required to fit these lines satisfactorily. The values obtained are given in Table I. The unblended lines were fitted to a precision of 0.0036 cm^{-1} which, considering the remaining blends and the difficulty of maintaining a consistent calibration of the spectrum, was judged to be about the same as the measurement error.

Similar to the problem in $^2\Pi$ states,[32] it was found that the J-dependent centrifugal distortion of the spin orbit, $a_N\zeta_e d$, and the spin-rotation interaction could not be simultaneously determined. The K-dependent distortion $a_K\zeta_e d$ could, however, be found simultaneously with ϵ_{aa}. We have named this term $a_K\zeta_e d$ by analogy with the other K-dependent distortion terms, rather than $a_D\zeta_e d$ as used by Endo, Saito, and Hirota.[15]

IV. DISCUSSION

The direct determination of the A rotational constants means that an improved calculation of the r_0 structure can be made. However, there are still only two pieces of data, B and A, and three structural parameters, R_{CH}, R_{Ca-C}, and θ_{HCH}. Most methyl compounds have C–H bond lengths near 1.10 Å. Taking this value with an estimated error of ± 0.02 Å gives the structural parameters in Table II.

The Ca–C bond length in monomethyl calcium is substantially longer (by 0.1 Å) than in calcium acetylide.[33] This is consistent with a much weaker metal–carbon bond strength. The main difference between the two species is the electron affinity of the anion ($E_A = 0.08$ eV for CH_3 (Ref. 34) and $E_A = 2.94$ eV for CCH (Ref. 35)]. This is very important in the alkaline earth free radicals because these molecules dissociate to the neutral species but are mainly ionic at the equilibrium internuclear distance. The small electron affinity for $CaCH_3$ means that the bond dissociation energy is small (< 45 Kcal mol^{-1} from the observed breakoff in fluorescence[12]). A longer Ca–C bond length is, therefore, to be expected.

In all of the calcium derivatives studied previously there was a decrease observed in the metal–ligand bond length upon excitation to the $\tilde{A}$ electronic state, typically by 0.02 Å. This is not the case for $CaCH_3$, indeed Table III shows a small increase; but if the C–H bond length were to have increased slightly (by as little as 0.01 Å), then there would be no increase upon excitation. In the absence of data for $CaCD_3$, no definite information is available, although the available data suggests that a decrease similar to that for the other calcium derivatives is unlikely.

Similar problems exist in interpreting the change in the A rotational constant. If the C–H bond length is assumed not to change, then an increase in the H–C–H bond angle of 3.6° is found. This is the most likely explanation for the change in A because it is consistent with the fairly large Franck–Condon factors for the methyl umbrella mode.[12] The frequency of this mode also decreases from 1085 to 1048 cm^{-1} on excitation to the $\tilde{A}\,^2E$ electronic state.[12]

From the values of A and $A\zeta_l$ in Table I, we find $\zeta_l = 0.976$. This is the total angular momentum about the top axis including orbital and vibrational contributions. The

TABLE I. Molecular constants for the 0_0^0 band of the $\tilde{A}\,^2E$–$\tilde{X}\,^2A_1$ system of $CaCH_3$ (in cm^{-1}).

	Constant	$\tilde{X}\,^2A_1$	$\tilde{A}\,^2E$
	T	···	14 743.1739(7)[a]
	$a\zeta_e d$	···	73.126 26(33)
10^4	$a_K\zeta_e d$	···	− 8.86(17)
	$A\zeta_l$	···	5.255 63(63)
10^5	$\eta_e\zeta_l$	···	3.522(24)
10^4	$\eta_K\zeta_l$	···	2.925(16)
10^{10}	$\eta_{eN}\zeta_l$	···	− 3.97(30)
10^8	$\eta_{KN}\zeta_l$	···	− 1.477(81)
	A	5.448 31(63)	5.384 14(63)
	B	0.252 376 6(22)	0.254 261 9(22)
10^5	D_K	7.03[b]	6.437(17)
10^5	D_{NK}	1.9624(52)	1.2980(52)
10^7	D_N	3.5381(41)	3.6203(41)
10^{10}	H_{KN}	6.05(85)	···
10^{10}	H_{NK}	3.608(92)	1.816(92)
	ϵ_{aa}	···	− 0.402 46(12)
	$(\epsilon_{bb} + \epsilon_{cc})/2$	0.001 821 8(44)	0.020 592(68)
10^5	D_{KS}	···	9.26(20)
10^5	D_{KNS}	···	1.592(45)
	ϵ_1	···	− 0.024 941(12)
10^5	ϵ_{1K}	···	− 6.88(31)
10^8	ϵ_{1N}	···	6.99(39)
10^4	h_1	···	1.6349(86)
10^7	h_{1K}	···	7.53(29)
10^9	h_{1N}	···	− 2.14(23)
	$5h_2 + \epsilon_{2b}$	···	± 0.001 178(44)

[a] One standard deviation error in parentheses.
[b] Held fixed; see text.

TABLE II. Molecular structure for the ground vibrational levels of the $\tilde{A}\,^2E$ and $\tilde{X}\,^2A_1$ states of $CaCH_3$.

Parameter	$\tilde{X}\,^2A_1$	$\tilde{A}\,^2E$
R_{CH} (Å)	1.100(20)[a]	1.100(20)
R_{CaC} (Å)	2.349(13)	2.353(14)
θ_{HCH} (deg)	105.6(28)	109.2(30)

[a] Estimated error in parentheses.

TABLE III. Some metal–carbon bond lengths for gas-phase dimethyl, trimethyl, and tetramethyl metal molecules.

Molecule	R_{M-C} (Å)	Molecule	R_{M-C} (Å)
$Be(CH_3)_2$ [a]	1.698	$B(CH_3)_3$ [b]	1.578
$Zn(CH_3)_2$ [c,d]	1.939	$Al(CH_3)_3$ [e]	1.957
$Cd(CH_3)_2$ [c]	2.112	$Sn(CH_3)_4$ [f]	2.144
$Hg(CH_3)_2$ [c,g]	2.094	$Pb(CH_3)_4$ [h]	2.238

[a] Reference 38.
[b] Reference 42.
[c] Reference 39.
[d] Reference 40.
[e] Reference 43.
[f] Reference 44.
[g] Reference 41.
[h] Reference 45.

spin-orbit constant $a\zeta_e d$ was found to be 73.1 cm^{-1}. The value for the corresponding $\tilde{A}\,^2\Pi$ state of CaCCH (Ref. 33) is 70.5 cm^{-1}, while the isoelectronic species CaF (Ref. 1) and CaOH (Ref. 8) have spin-orbit constants of 71.5 and 66.8 cm^{-1}, respectively. The value of $a\zeta_e d$ for $CaCH_3$ is the largest of all these, suggesting that both ζ_e and d are very close to 1.

The $\tilde{A}\,^2E$ state of $CaCH_3$ arises from a mixture of Ca^+ $3d\pi$ and $4p\pi$ configurations. An additional ^2E state arising from the $3d\delta$ configuration must also be present within a few thousand wave numbers of the $\tilde{A}\,^2E$ state. This state corresponds to a $^2\Delta$ state in cylindrical symmetry and can have $\zeta_e = 2$. This state (which we shall call $\tilde{A}'\,^2E$) and the $\tilde{A}\,^2E$ state can mix and possibly give ζ_e slightly greater than 1 for the $\tilde{A}\,^2E$ state.

The Jahn–Teller quenching parameter d must still be very close to 1; however, it is consistent with a very small Jahn–Teller interaction.

Hougen[29] has derived a series of expressions relating the spin-rotation and Λ-doubling-type terms to interactions with other electronic states. The two Λ-doubling-like terms which are related to the diatomic molecule p and q parameters ($\epsilon_1 = p/2$, $h_1 = -q/2$), are given by

$$h_1 = B^2\Big(\sum_i |\langle A^i|L_-|E^0_+\rangle|^2/\Delta E_{0i} - \sum_i |\langle A^i_1|L_-|E^0_+\rangle|^2/\Delta E_{0i}\Big),$$

$$\epsilon_1 = -(a_\perp/B)h_1.$$

A reasonable approximation can be made by considering the interaction only between the $\tilde{A}\,^2E$ state and the $\tilde{B}\,^2A_1$ state. If these are treated as pure p states, then the expression for h_1 reduces to

$$h_1 = -B^2 l(l+1)/\Delta E_{AB} = -2B^2/\Delta E_{AB}.$$

From the low-resolution work $\Delta E_{AB} = -1260\ cm^{-1}$, which gives

$$h_1 = 1.0\times 10^{-4}\ cm^{-1},$$

compared with the observed $h_1 = 1.6\times 10^{-4}\ cm^{-1}$. If $a_\perp$ is taken as $a\zeta_e d = 73\ cm^{-1}$, then we find

$$\epsilon_1 = a_\perp Bl(l+1)/\Delta E_{AB} = -0.030\ cm^{-1}$$

compared with the observed $\epsilon_1 = -0.025\ cm^{-1}$. Both values are in reasonable agreement considering the approximations made. These calculations use the polyatomic version of the simple "pure procession"[36] relationships widely used by diatomic molecule spectroscopists.[37]

$CaCH_3$ is the first example from the family of monomethyl metal molecules to be characterized by high-resolution spectroscopy. Some metal–carbon bond lengths are available for gas-phase dimethyl, trimethyl, and tetramethyl metal compounds from electron diffraction and Raman studies.[38–45] A collection of metal–carbon bond lengths are provided in Table III for comparison purposes.

V. CONCLUSION

A full rotational analysis of the 0^0_0 band of the $\tilde{A}\,^2E$–$\tilde{X}\,^2A_1$ system has been carried out. The metal–ligand bond length was found to be significantly longer than in similar species, consistent with the low bond dissociation energy found earlier.

ACKNOWLEDGMENT

This research was supported by the National Science Foundation (Grant No. CHE-8608630).

[1] J. Nakagawa, P. J. Domaille, T. C. Steimle, and D. O. Harris, J. Mol. Spectrosc. **70**, 374 (1978).
[2] M. Dulick, P. F. Bernath, and R. W. Field, Can. J. Phys. **58**, 703 (1980).
[3] T. C. Steimle, P. J. Domaille, and D. O. Harris, J. Mol. Spectrosc. **68**, 134 (1977).
[4] T. C. Steimle, P. J. Domaille, and D. O. Harris, J. Mol. Spectrosc. **73**, 441 (1978).
[5] J. Nakagawa, R. F. Wormsbecher, and D. O. Harris, J. Mol. Spectrosc. **97**, 37 (1983).
[6] R. C. Hilborn, Zhu Qingshi, and D. O. Harris, J. Mol. Spectrosc. **97**, 73 (1983).
[7] P. F. Bernath and S. Kinsey-Nielsen, Chem. Phys. Lett. **105**, 663 (1984).
[8] P. F. Bernath and C. R. Brazier, Astrophys. J. **288**, 373 (1985).
[9] C. R. Brazier and P. F. Bernath, J. Mol. Spectrosc. **114**, 163 (1985).
[10] R. F. Wormsbecher, R. E. Penn, and D. O. Harris, J. Mol. Spectrosc. **97**, 65 (1983).
[11] C. R. Brazier and P. F. Bernath (in preparation).
[12] C. R. Brazier and P. F. Bernath, J. Chem. Phys. **86**, 5918 (1987).
[13] F. S. Pianalto, C. R. Brazier, A. M. R. P. Bopegedera, and P. F. Bernath (in preparation).
[14] G. W. King and C. H. Warren, J. Mol. Spectrosc. **32**, 138 (1969).
[15] Y. Endo, S. Saito, and E. Hirota, J. Chem. Phys. **81**, 122 (1984).
[16] L. C. O'Brien, C. R. Brazier, and P. F. Bernath, J. Mol. Spectrosc. **130**, 33 (1988).
[17] S. C. Foster, P. Misra, T.-Y. D. Lin, C. P. Damo, C. C. Carter, and T. A. Miller, J. Phys. Chem. **92**, 5914 (1988).
[18] X. Liu, C. P. Damo, T.-Y. D. Lin, S. C. Foster, P. Misra, L. Yu, and T. A. Miller, J. Phys. Chem. **93**, 2266 (1989).
[19] Y.-C. Hsu, X. Liu, and T. A. Miller, J. Chem. Phys. **90**, 6852 (1989).
[20] L. Yu, S. C. Foster, J. M. Williamson, M. C. Heaven, and T. A. Miller, J. Phys. Chem. **92**, 4263 (1988).
[21] T. Momose, Y. Endo, E. Hirota, and T. Shida, J. Chem. Phys. **88**, 5338 (1988); **90**, 4636(E) (1989).
[22] Y. Endo, S. Saito, and E. Hirota, J. Chem. Phys. **85**, 1770 (1986).
[23] J. B. West, R. S. Bradford, J. D. Eversole, and C. R. Jones, Rev. Sci. Instrum. **46**, 164 (1975).
[24] S. Gerstenkorn and P. Luc, *Atlas du Spectre d'Absorption de la Molecule d'Iode* (Laboratorie Amie-Cotton, CNRS 9145, Orsay, France, 1978).
[25] S. Gerstenkorn and P. Luc, Rev. Phys. Appl. **14**, 791 (1979).
[26] G. Herzberg, *Electronic Spectra and Molecular Structure of Polyatomic Molecules* (Van Nostrand-Reinhold, New York, 1966), pp. 84–99.
[27] J. T. Hougen, J. Chem. Phys. **37**, 1433 (1962).
[28] J. M. Brown, Mol. Phys. **20**, 817 (1971).
[29] J. T. Hougen, J. Mol. Spectrosc. **81**, 73 (1980).
[30] G. Graner, Mol. Phys. **31**, 1833 (1976).
[31] This material is available through the Physics Auxiliary Publication Service. See AIP document No. PAPS JCPAS-91-4548-64 for 64 pages of measured line positions of the 0^0_0 band of the $\tilde{A}\,^2E$–$\tilde{X}\,^2A_1$ transition of $CaCH_3$. Order by PAPS number and journal reference from the American Institute of Physics, Physics Auxiliary Publication Service, 335 East 45th Street, New York, NY 10017. The price is $1.50 for each microfiche (98 pages) or $5.00 for photocopies up to 30 pages, and $0.15 for each additional page over 30 pages. Airmail additional. Make checks payable to the American Institute of Physics.
[32] J. M. Brown and J. K. G. Watson, J. Mol. Spectrosc. **65**, 65 (1977).
[33] A. M. R. P. Bopegedera, C. R. Brazier, and P. F. Bernath, J. Mol. Spectrosc. **129**, 268 (1988).
[34] G. B. Ellison, P. C. Engelking, and W. C. Lineberger, J. Am. Chem. Soc. **100**, 2556 (1978).
[35] B. K. Janousek, J. I. Brauman, and J. Simons, J. Chem. Phys. **71**, 2057 (1979).

[36]R. S. Mulliken and A. Christy, Phys. Rev. **38**, 87 (1931).
[37]H. Lefebvre-Brion and R. W. Field, *Perturbations in the Spectra of Diatomic Molecules* (Academic, Orlando, FL, 1986).
[38]A. Almenningen, A. Haaland, and G. L. Morgan, Acta Chem. Scand. **23**, 2921 (1969).
[39]K. S. Rao, B. P. Stoicheff, and R. Turner, Can. J. Phys. **38**, 1516 (1960).
[40]A. Almenningen, T. U. Helgaker, A. Haaland, and S. Samdal, Acta Chem. Scand. Ser. A **36**, 159 (1982).
[41]K. Kashiwabara, S. Konaka, T. Iijima, and M. Kimura, Bull. Chem. Soc. Jpn. **46**, 407 (1973).
[42]L. S. Bartell and B. L. Carroll, J. Chem. Phys. **42**, 3076 (1965).
[43]A. Almenningen, S. Halvorsen, and A. Haaland, Acta Chem. Scand. **25**, 1937 (1971).
[44]M. Nagashima, H. Fujii, and M. Kimura, Bull. Chem. Soc. Jpn. **46**, 3708 (1973).
[45]T. Oyamada, T. Iijima, and M. Kimura, Bull. Chem. Soc. Jpn. **44**, 2638 (1971).